JOURNAL OF SOLID STATE CHEMISTRY 109, 152–165 (1994)

Defects and Phase Transition in Monoclinic Natural Hollandite: $Ba_xMn_8O_{16}$

L. C. Nistor,[1] G. Van Tendeloo, and S. Amelinckx[2]

University of Antwerp (RUCA), Groenenborgerlaan 171, B 2020 Antwerp, Belgium

Received May 17, 1993; accepted July 14, 1993

Needles of natural hollandite $Ba_xMn_8O_{16}$ were examined by electron diffraction and high-resolution electron microscopy. This material was found to adopt the monoclinic structure, space group $I2/m$, with a_m = 1.024 nm, b_m = 0.29 nm, c_m = 0.98 nm, β = 92.5°. The distribution of the barium ions in the channels was directly visualized and showed a preferential separation of $2b_m$. The structure was found to show many defects. The main defects present were crystallographic shear planes. The uniform arrangement of these planar defects leads to structural variants, which in some cases produced incommensurate diffraction patterns. Transition from the monoclinic to the tetragonal phase was observed at a temperature around 330°C. The cooling to the monoclinic phase suggests that the deformation of the MnO_6 octahedra, which apparently determines the monoclinic deformation, can occur in two different ways, producing twin related structures.

1. INTRODUCTION

The hollandite family of compounds has been the subject of intense structural research in recent years because of its possible use as a stable host material for radioactive ions from nuclear wastes (1–4). It was suggested in particular that certain synthetic hollandite structures such as $A_xM(IV)_{4-x}N(III)_{2x}O_8$, where A = Sr, Ba; M = Ti, Sn; N = Al, Cr, Ga, In (5), might accommodate in a stable way radionuclides in the channels of the structure. As a result, most of the attention was devoted to the arrangement and mobility of different types of ions in the channels of these structures (6–11). Much less attention was devoted to the structure of the generic compound of the family: the mineral hollandite $Ba_xMn_8O_{16}$.

In this paper we report on a study of the defect structure of a natural hollandite, originating from an unknown locality in Arizona (USA). The hollandite forms a coating of very fine, millimeter long, shiny, black needles on a massive black rock, probably consisting of mixed manganese oxides.

The structural features were found to be different from those of the synthetic materials. Moreover, the improvements in the quality of high-resolution images, achievable with present-day microscopes, has allowed us for the first time to image the structure with a resolution of approximately 0.16 nm, making directly visible all heavy atom columns in the structure. Also, the distribution of the barium ions in the channels could be visualized directly. Moreover, it was found that superstructures, due to ordered planar defects, occur in the manganese framework, leading in a number of cases to incommensurate electron diffraction patterns.

Finally, it is shown that the monoclinic deformation disappears at temperatures above approximately 330°C, where the symmetry becomes tetragonal.

2. STRUCTURAL CONSIDERATIONS

The structure of the mineral hollandite was first described by Byström and Byström (12), and was subsequently refined (13, 14).

Assuming a somewhat simplified reference composition $Ba_xMn_8O_{16}$, the structure can be described as consisting of layers of partially edge-sharing and partially corner-sharing MnO_6 octahedra. This gives rise to a planar network forming a crossed grid of interlinked MnO_6 double chains parallel to the layer normal. One layer is represented schematically in Fig. 1.

The double chains of edge-sharing octahedra are parallel to the b-direction of the monoclinic cell with lattice parameters a = 1.0 nm, b = 0.287 nm, c = 0.973 nm, β = 91°. Within each chain, the octahedra share opposite edges in the b-direction. The crossed grid leaves rather large roughly square-shaped channels which can be occupied by Ba ions. Only a fraction of the equivalent interstitial sites within these channels is occupied, leading to a variable stoichiometry. In the structure, the layers such as the one shown in Fig. 1 are stacked vertically.

From the electron microscopic point of view, the struc-

[1] Permanent address: Institute of Atomic Physics, P.O. Box Mg.6, Magurele, 76900 Bucharest, Romania.

[2] To whom correspondence should be addressed.

0022-4596/94 $6.00

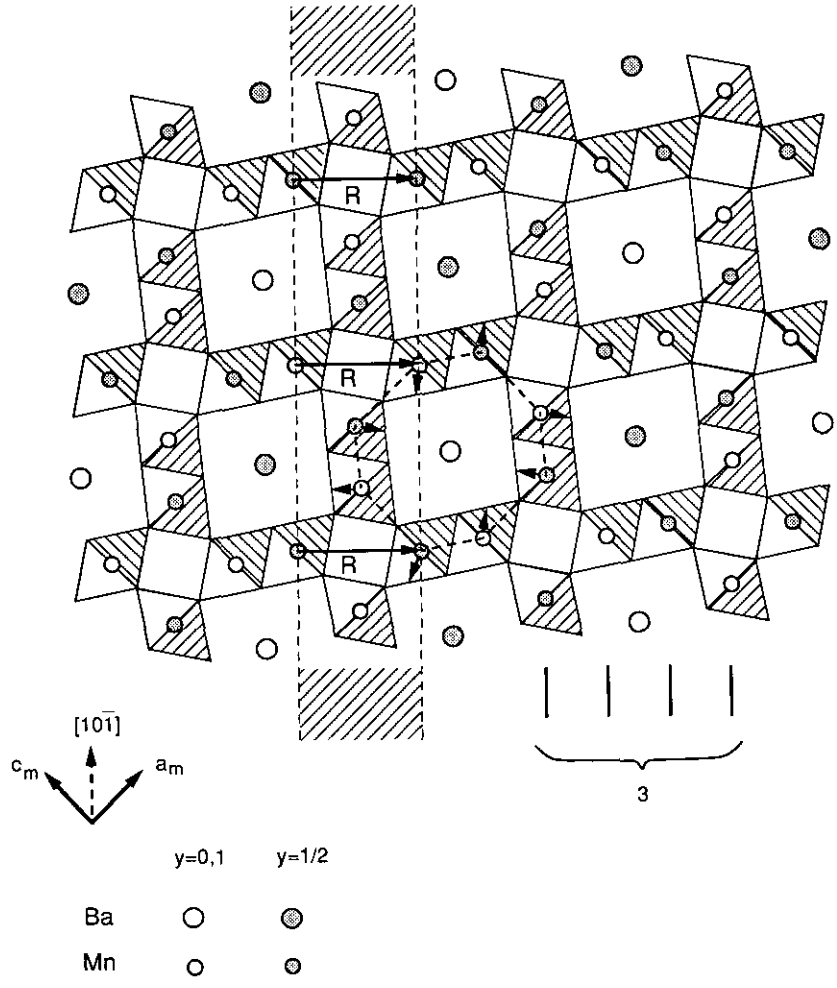

FIG. 1. Schematic representation of the monoclinic hollandite structure projected on (010). The manganese columns form a slightly deformed octagon, while the barium columns form a parallelogram-shaped lattice with a mesh of 0.71 × 0.69 nm.

ture is an ideal "column" structure when viewed along the *b*-axis; all columns are well separated and contain one type of atoms only. This is directly related to the shortness of the *b*-axis.

Whereas the structure was originally described as body centered tetragonal (12) with $a = 0.98$ nm and $c = 0.286$ nm (space group C_{4h}^5–$I4/m$) it was soon realized that the structure has, in fact, a body-centered monoclinic space group C_{2h}^3–$I2/m$, with the above-mentioned parameters. The monoclinic symmetry was shown to result from a deformation and rotation of the MnO_6 octahedra. The deformation can be described as a coupled rotation of the double chains, as represented schematically in Fig. 1 according to (15). As a result of the deformations and the associated atom displacements, the square channel is deformed into a slightly smaller, lozenge-shaped one. Only the octahedra on opposite walls of the channel remain identical, reducing the fourfold axis to a twofold one. The dimensional characteristics of the channels are thus controlled by the octahedra deformations (1), which in turn depend on the channel ions.

The same displacement pattern, which has twofold rotation symmetry, can be applied to the tetragonal model, after a 90° rotation, which is a symmetry operation for this model. The two resulting monoclinic structures are equivalent but related by a 90° rotation. A consideration of the point groups leads to the same conclusion. The point group of the monoclinic structure is $2/m$; it is a subgroup of the point group of the tetragonal structure $4/m$ with parallel twofold and fourfold axes. This relationship suggests that the monoclinic structure could be formed by a phase transition from the tetragonal phase, which then would be the stable phase at high temperature. The resulting variants would then be related by the lost symmetry operation, i.e., by a 90° rotation about the fourfold axis.

As viewed along the *b*-axis the manganese columns form a slightly deformed elongated octogon, the direction

of the elongation being along the a-axis. In the same view the barium columns form a lattice with a parallelogram-shaped mesh of 0.71 nm × 0.69 nm and an angle of 91°.

3. EXPERIMENTAL

Optical microscopy observations showed that, as is usual for minerals, the sample consists of different oxide phases showing several morphologies and shapes. Under the optical microscope only the black needles were chosen, which were subsequently gently crushed to obtain areas transparent to the electron beam. The double tilt and heating stages of the Phillips CM-20 electron microscope were used, respectively, for inspecting the reciprocal space, and for heating the sample to study the monoclinic to tetragonal phase transition. High-resolution images were obtained with the JEOL-4000EX electron microscope at an accelerating voltage of 400 kV.

4. OBSERVATIONS

4.1. Diffraction Patterns

In this section we give a description of the observed diffraction patterns; the interpretation is discussed in Section 5, after we have described the high-resolution images.

The reciprocal lattice of the compound was found to be consistent with a monoclinic body-centered lattice with the parameters $a_m = 1.024$ nm, $b_m = 0.29$ nm, $c_m = 0.98$ nm, $\beta = 92.5°$, although some variability was noticed among different needles. This can be deduced from the set of diffraction patterns reproduced in Fig. 2. They represent the [010], [100], [$1\bar{1}0$], and [$11\bar{1}$] zones, respectively. In Fig. 2c the ($1\bar{1}0$)* section of the reciprocal space has been obtained by tilting slightly away from the a-zone (Fig. 2b) around the c*-direction. Figure 2a allows us to measure directly the a_m and c_m parameters, and the β angle, while from Fig. 2b the b_m parameter can be deduced. We further note that only spots with $h + l = 2n$ are present. Since the reciprocal monoclinic unit cell is all face centered, the unit cell of the monoclinic cell is body centered.

Although body-centered monoclinic space groups are unconventional and do not appear in the "International Tables," we continue to use this description because the deviation from the body-centered tetragonal is small, and also for historical reasons.

The diffraction pattern along the [010] zone of Fig. 2a shows that twinning occurred in certain crystals. The complex pattern results from the superposition of two single-crystal patterns after a relative rotation over approximately 90° about the [010] axis, which is a pseudo-symmetry operation since the structure is close to tetragonal. There is no well-determined line of unsplit spots, as would be the case for coherent reflection twins.

In sections of Figs. 2b and 2c diffuse lines are present perpendicular to the [010] direction. Very weak lines coincide with the dense row of spots; somewhat less weak lines and sharp lines are situated midway between the dense row of spots. Tilting experiments have demonstrated that these lines are the intersections of Ewald's sphere with planes of diffuse intensity situated in (010)* planes and corresponding to an interatomic separation of $2b_m$.

However, the most striking diffraction patterns are reproduced in Fig. 3a. The zone axis is [010], i.e., the same as in Fig. 2a. The pattern from Fig. 3a is clearly incommensurate along the [101]* direction. The most prominent reflections are the third-order reflections, indicated by arrowheads; they form a two-dimensional lattice with a mesh size 3[101]* × [$10\bar{1}$]*. All the other reflections along the dense rows can be considered as satellite reflections of these prominent ones, suggesting the presence of a one-dimensional modulated structure. The length of the q-vector of the modulation, indicated by the arrowhead closest to the central spot and expressed as a fraction of the distance between the strong spots, is 0.29, whereas the interplanar spacing corresponding with the first-order prominent reflection is 0.24 nm. This interplanar distance is approximately one-third of the interplanar distance along the same direction in the normal structure (Fig. 2a). The nature of this modulation becomes clear after we have discussed the high-resolution images.

The [010] diffraction pattern of Fig. 3c exhibits weak streaks along the [101] direction passing through the row of equidistant spots parallel to that direction. Every third row of spots along the [101]* direction has remained sharp and round; all other spots are elongated and become streaked. This observation is consistent with the presence of a random distribution of planar defects which, as is shown later, can be described as crystallographic shear planes.

Figure 3b shows a somewhat similar diffraction pattern. However, the rows of streaked spots are no longer equidistant. The two rows of streaked spots situated between two sharp spot rows are more widely separated. The succession of spacings between two spots as fractions of the separation of the main sharp spots is 7/22; 8/22; 7/22. As in Fig. 3a this pattern is due to a modulated structure, but is poorly ordered, the q-vector being 7/22. No satellite spots are visible because of this disorder.

4.2. High Resolution Images

The [010] zone, high-quality, high-resolution image of Fig. 4, obtained from the thinnest part of the specimen, reveals all the heavy atom columns as dark dots. The elongated shape of the octagon of manganese columns, surrounding columns of barium ions, can be clearly recog-

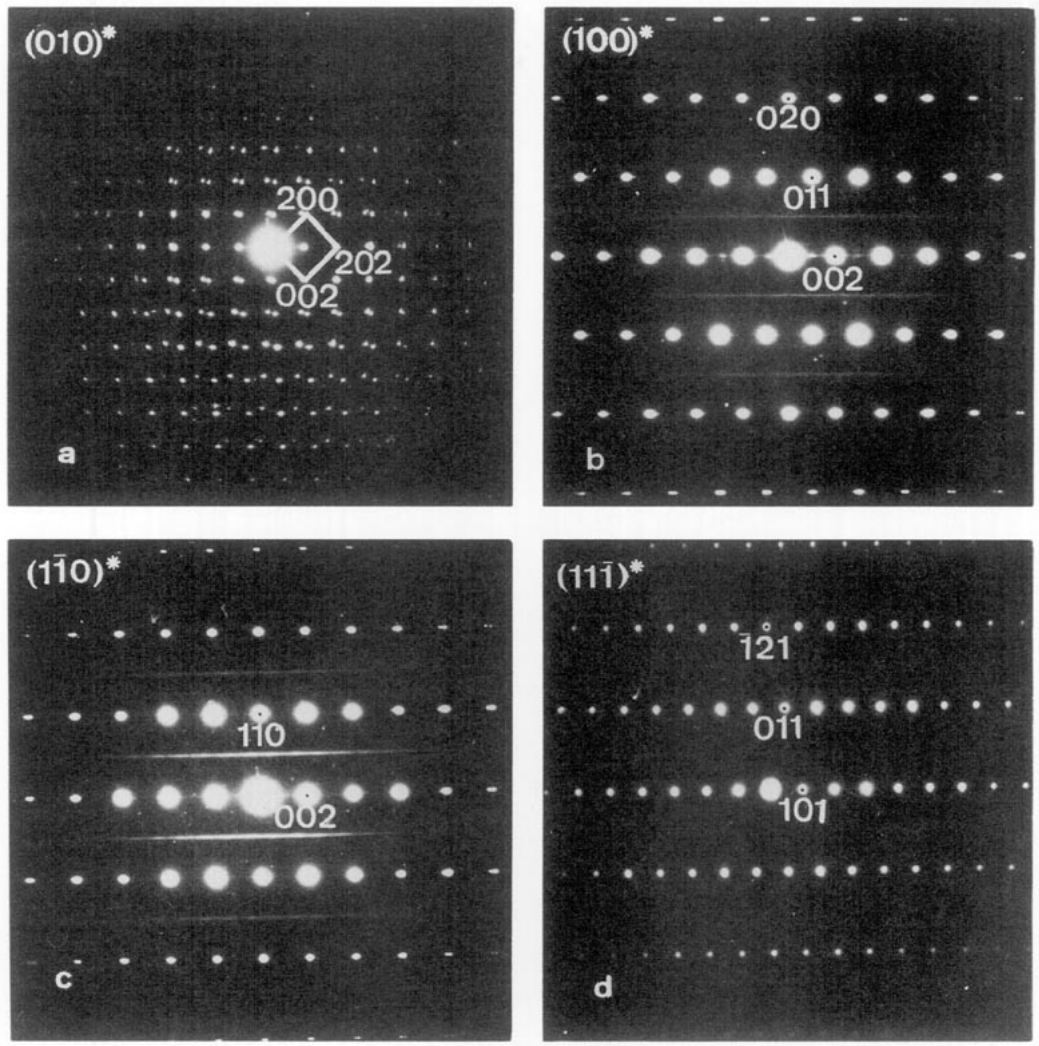

FIG. 2. Four sections of the reciprocal space of the basic structure: (a) (010)* section; (b) (100)* section; (c) (1$\bar{1}$0)* section; (d) (11$\bar{1}$)* section.

nized; this confirms the displacement pattern as described in (15). The image can be compared with the model of the structure given in Fig. 1. The interpretation of the image is unambiguous, even without comparing it with simulated images, because of the different abundancies of barium and manganese, and because of their characteristic geometrical features. Not only the shape of the black dot pattern, but also the scale is completely in accordance with the structure determination. Oxygen atoms are not revealed as separate columns.

An interesting type of planar defect, visualized as a row of elongated, almost rectangular meshes is indicated by an arrow in Fig. 4. The image allows us to propose a model. In the normal structure the channels are almost square, lozenge shaped, and the four channel walls consist of double chains of edge-sharing octahedra as shown in Fig. 1. Each channel is occupied by one string of barium ions. Along the defect, a layer consisting of almost-rectangular, parallelogram-shaped channels is present. Two opposite channel walls now consist of triple chains of octahedra, whereas the two remaining opposite walls consist of double chains, as before. The structure of such a layer is represented schematically in Fig. 5a. The central channel is now parallelogram shaped and there is room for two strings of barium ions in a staggered configuration. The heavy atom columns proposed in this model can be observed as dark dots in their correct configurations and on the right scale in Fig. 4. A compound which would only contain layers of this type would have the composition $Ba_{2-x}Mn_5O_{10}$, if the barium configuration would be kept unchanged, i.e., it would contain more barium than the normal structure. However, this is unrealistic and it clearly depends on the occupancy of the double channel. The nonequivalence in shade of the two dots within the parallelogram-shaped channel with those present in the "square" channels suggest that their degree of occupancy

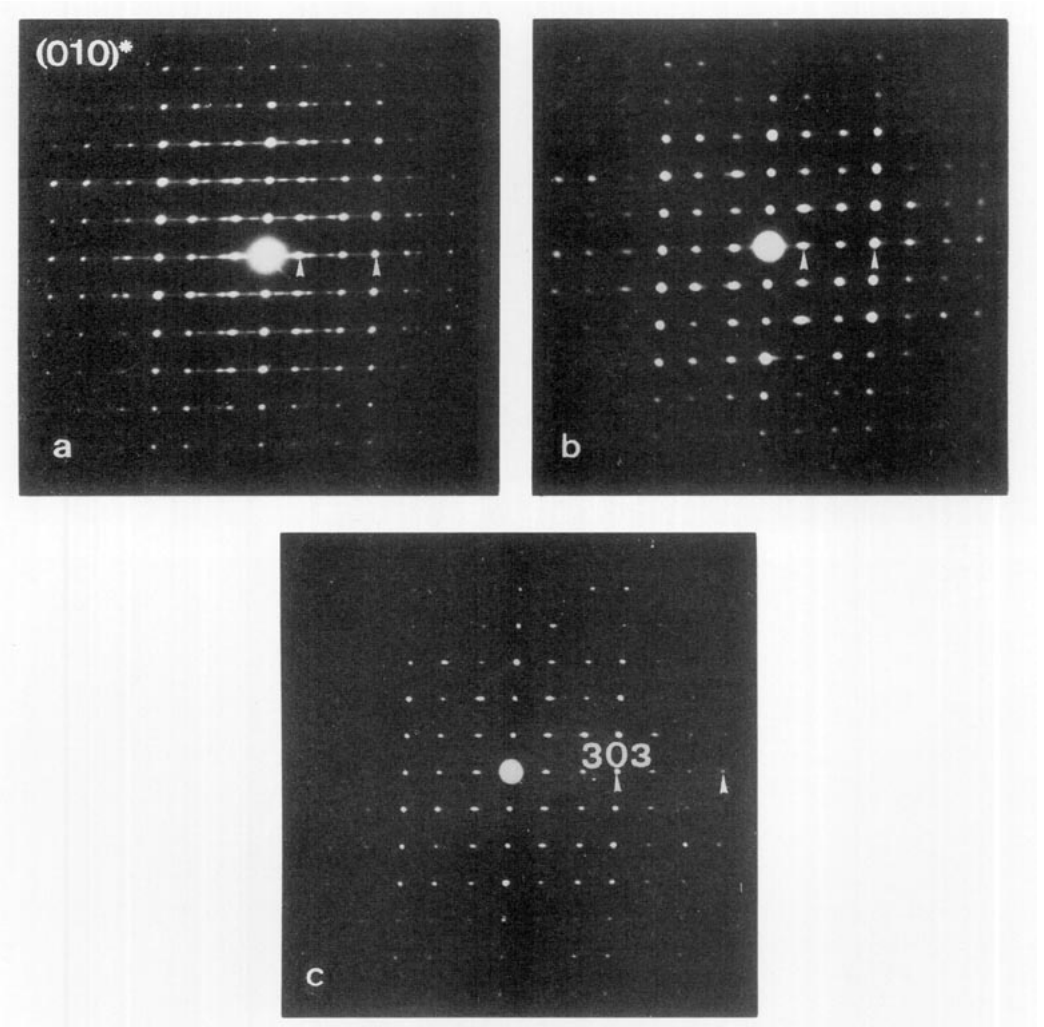

FIG. 3. Diffraction patterns with [010] zone axes corresponding to different faulted parts of the sample: (a) incommensurate by modulated along [101]* direction, $q = 0.29$; arrowheads indicate the end point of the q vector and the strong spots; (b) incommensurate by modulated, $q = 0.32$; arrowheads have the same significance as in (a); (c) streaked; arrowheads indicate the sharp round spots.

is smaller, in accordance with a staggered configuration, maintaining the same average separation as in the single channels. The presence of the defects can therefore be considered as a way of accommodating a smaller barium content for the same MnO_2 content.

We note that, whereas in the normal structure the repeat period along [101] contains three rows of MnO_6 octahedra, the defected lamella contains four such rows. This is schematically indicated in Fig. 5a.

The planar defect is in fact a "crystallographic shear plane" which appears when the structure has to accommodate nonstoichiometry (16). It can be described in the following manner: We remove the cross-hatched band indicated in Fig. 1 and close the gap caused by doing so, by a relative displacement over **R** of the two crystal parts. It is clear that the resulting defect is the one discussed above. The shear operation is conservative as far as the MnO_2 sublattice is concerned, since complete octahedra are removed, but it would increase the barium content, if the barium configuration would remain unchanged. Since we have removed a lamella with a thickness of $(\frac{2}{3})d_{101}$, the width of the band becomes $(\frac{4}{3})d_{101}$. The width ratio of the two blocks is thus 4 : 3. The distribution of these planar defects over the sample is mostly random, but in small areas a periodic distribution was sometimes observed.

Figure 6 shows a high-resolution image of roughly rectangular intersections of such crystallographic shear planes. In this case, if we image the same "cut and displace" model as previously (Fig. 1), but in the perpendicular direction, we obtain a linear defect as represented schematically in Fig. 5b. All the walls of the channel are formed by triple chains of MnO_6 edge-sharing octahedra. This channel is clearly larger than the rectangular ones.

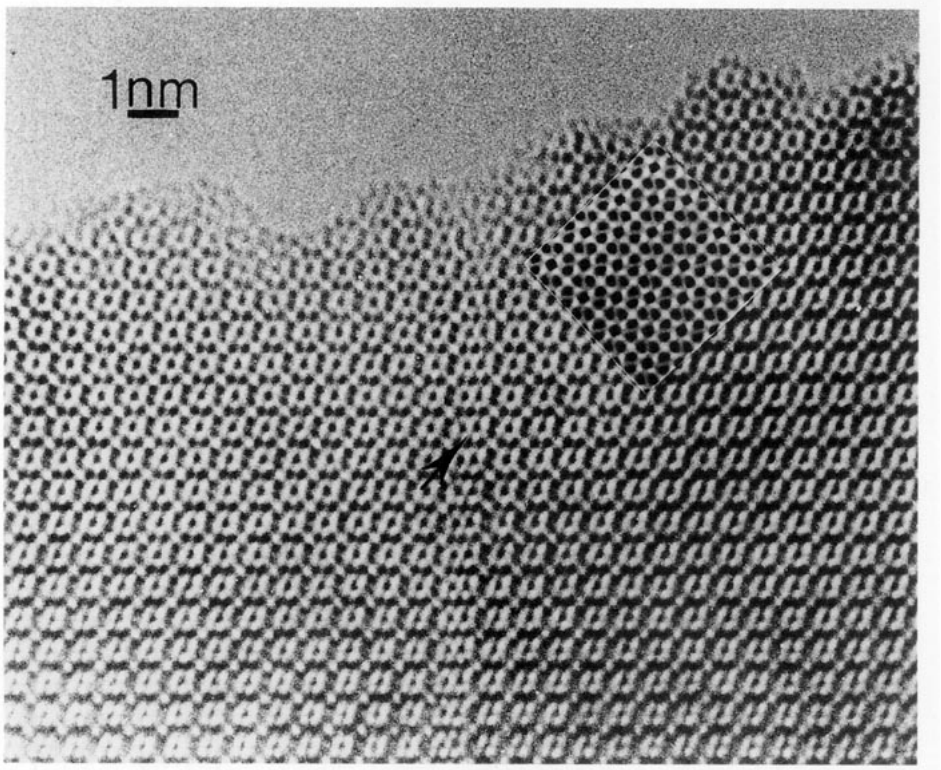

FIG. 4. High-resolution image along the [010] zone. The interface is a crystallographic shear plane. The simulated image is shown as inset.

The high-resolution image exhibits four dots within the channel, suggesting that the barium ions occur in four columns parallel to the [010] direction. At a given level these columns cannot all be fully occupied since the separation between barium ions would then become too small. Energetically, the most favorable barium configuration consists in a helical arrangement, maximizing the average separation for a given occupancy level. Along any one of the four columns, only roughly one in three or four potential sites are occupied, since this leads to the same average distance as along the single channels.

Also, in Fig. 6 a complex dislocation is visible in D. The dislocation is sessile and of the Frank type. Although the dislocation is not dissociated in the usual sense, it has a complicated core structure. Along two mutually perpendicular directions, indicated by arrowheads in Fig. 6, a rectangular channel layer becomes a layer of single channels.

The image of Fig. 7 along the $[11\bar{1}]$ zone, which is nearly perpendicular to the channel axis, reveals indirectly the occupation of the channels. The most favorable orientation to image the geometry of the barium atoms along the channel is $[11\bar{1}]$, since along this zone the barium ions form the most densely packed, well-separated columns. Moreover, because of the small b_m parameter, the $[11\bar{1}]$ direction forms an angle close to 90° with the channel direction. The actual separation of the barium ions is thus almost conserved. Half of the manganese atoms form columns along this zone, the other half being projected as columns of close pairs of atoms. These two types of columns are imaged as dots with a different brightness, as is clear from Fig. 7 and from the simulated image (Fig. 12). On the other hand the barium atom columns are imaged as dark areas indicated by arrowheads. The marked difference in contrast behavior between manganese and barium is a consequence of the large difference in atomic number.

The high-resolution image shows dot rows of three different gray levels, leading to a period of 0.705 nm. Along the rows the period is approximately 0.287 nm, which is equal to the thickness of one (010) layer. Every third row contains prominently black dots with a double interdot spacing, i.e., 0.574 nm. Occasionally an isolated triple spacing causes a longitudinal shift of the array of black dots within that row. In adjacent rows the black dots are shifted over $(\frac{1}{2})b_m$; the shift tends to occur systematically in the same sense in successive rows, leading to a parallelogram-shaped black dot lattice. Occasionally the shift occurs in the opposite sense. The dots presumably do not represent individual barium ions, but reveal the coincidence pattern of barium ions in superimposed rows. The darker dots in a row are usually spaced by $2b_m$, whereas

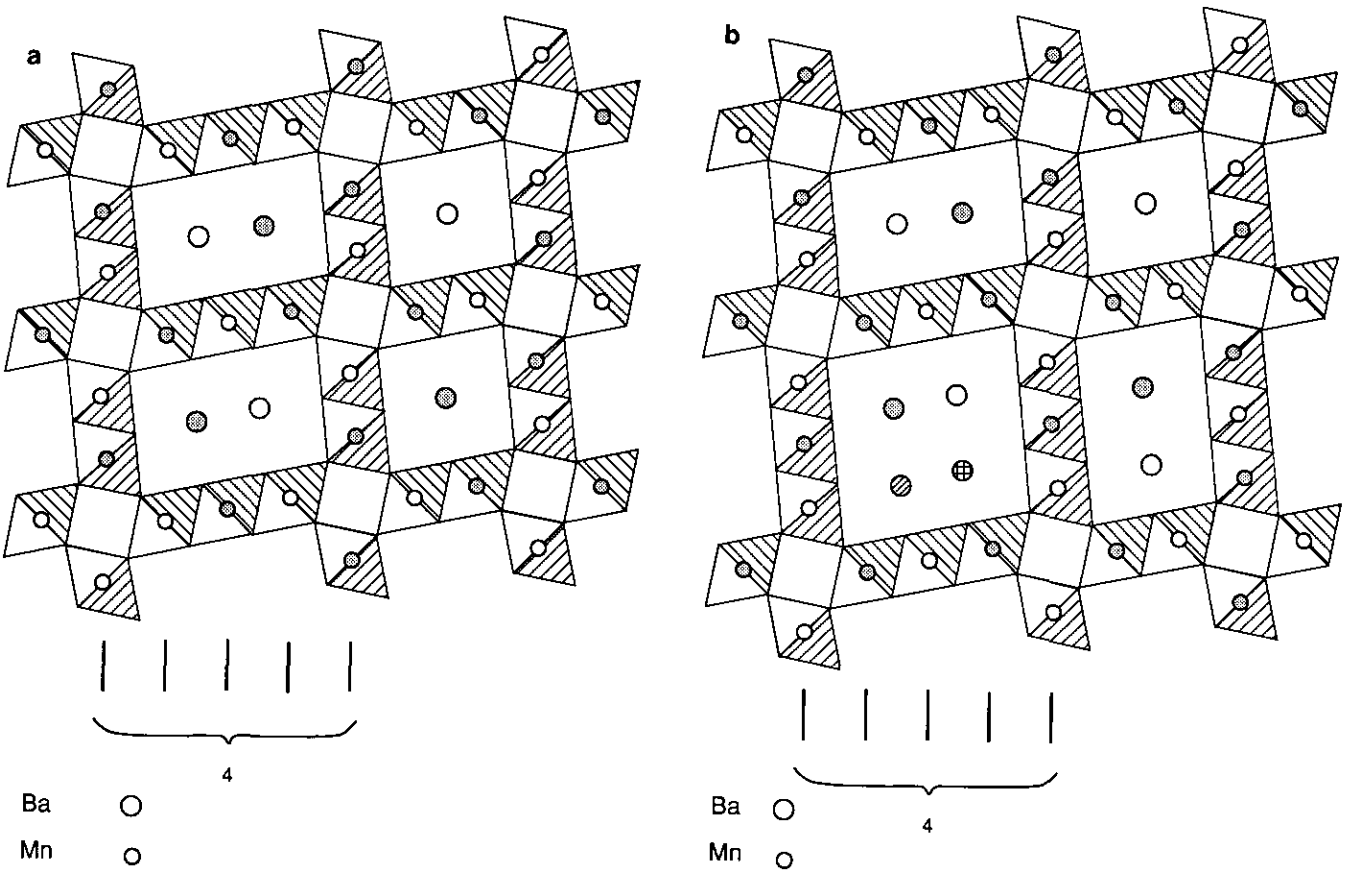

FIG. 5. Schematic representation of a crystallographic shear plane: (a) one planar defect; (b) two mutually perpendicular planar defects.

in the same row, often less dark dots are spaced by b_m only, as, for instance, in Fig. 7 (arrowheads). The intense black dots spaced by $2b_m$ are produced when coincidence occurs along the viewing direction in several overlapping channels. This is represented schematically in Fig. 8a. On the other hand, medium black dot sequences with a spacing b_m occur when both projected positions are almost equally occupied. This is represented schematically in Fig. 8b. The brightness variation of these dark dot sequences reflects the preference of Ba ions for a $2b_m$ separation along the channels, and shows, at the same time, that the relative positions of the barium strings in neighboring rows are not strictly correlated.

5. INTERPRETATION

5.1. Polytypoids; Shear Structures

The presence of two different block sizes, the normal size S and the larger size L, in the ratio $S/L = \frac{3}{4}$ makes it possible to imagine composition-driven polytypoids or shear structures, as well as pseudo-incommensurate structures.

In Fig. 9a the structure is imaged in high resolution along the [010] zone. The sample is somewhat thicker and therefore the atomic resolution is not achieved. However, the regular succession of long (L) and short (S) blocks can nevertheless be recognized. The succession is clearly *LSSLSS* ..., whereas in Fig. 9b, it is ... *LSLSLS* .... The areas exhibiting such structural variants are usually too small to produce a well-characterized sharp electron diffraction patterns.

The incommensurate diffraction pattern of Fig. 3a, taken over a larger area, can be consistently interpreted in terms of a model based on a uniform mixture of the two types of observed blocks; no evidence was found for other block sizes. The high-resolution images have shown that sequences of two different lamellae with sizes L and S occur along the [101] direction. This suggests that the incommensurate diffraction pattern can be attributed to a sequence consisting of a complex but "uniform" mixture of these two block sizes. We show that this is indeed the case.

We note that the prominently bright diffraction spots in Fig. 3a occupy the positions of the third-order spots in the normal diffraction pattern (Fig. 2a). The same position

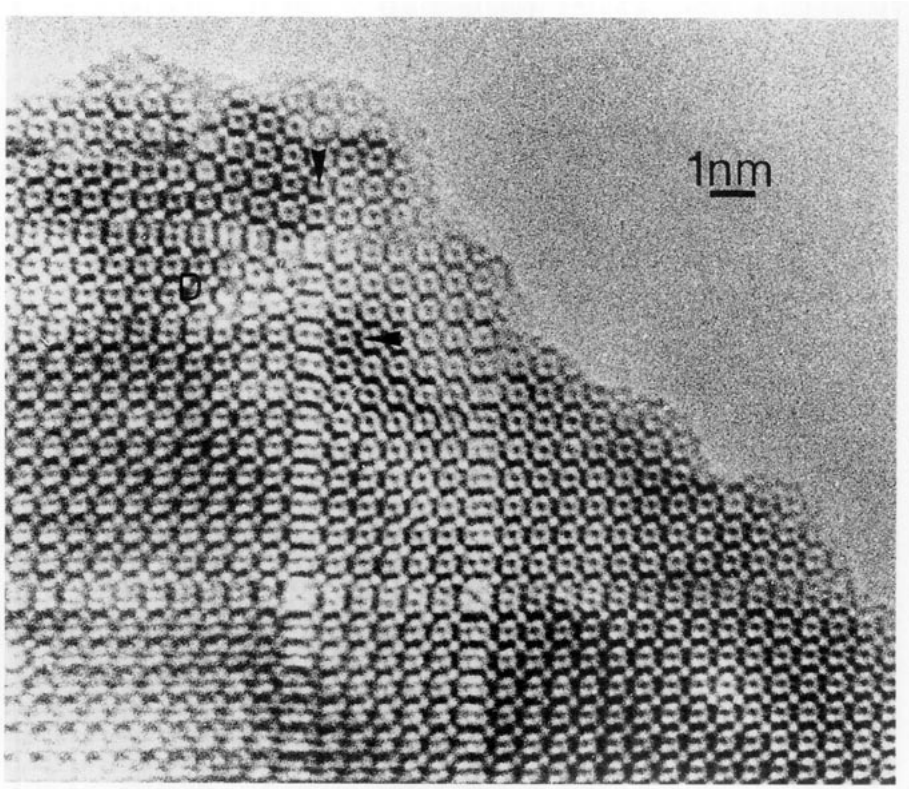

FIG. 6. High-resolution image along the [010] zone illustrating rectangular intersections of crystallographic shear planes. A dislocation marked D is also visible.

would also be occupied by the fourth-order spot, if the structure had contained only L blocks. As a fundamental building unit of the modulated structure we can therefore consider one-third of the size of an S block, which, within the experimental error, is equal to one-fourth of an L block. The ratio of the constituent lamella is thus rational, i.e., $L:S = 4:3$. The modulation period is $\lambda = 1/q = 3.45$, expressed in fundamental building units. A sequence having such an average period can always be constructed from a uniform mixture of lamellae with sizes equal to 3 and 4 building units. Uniform sequences which are the best approximation to equidistant sequences produce sharp spots. They can be derived using the algorithm described in (17), which is a variant of the "cut and projection" method (18). With $q = 0.29$, $L = 4$, and $S = 3$ this method leads to a slope $\phi = 44.5°$. The corresponding stacking sequence is found by the construction shown in Fig. 10a. It leads to the sequence ... *SSLSLSSL* ... or (... 33434334 ...).

Similarly, the corresponding block sequence which gave the diffraction pattern of Fig. 3b consists almost of purely 3-blocks, with an occasional apparition of a 4-block.

The method also allows us to predict semiquantitatively the kinematical diffraction pattern of such block sequences, provided the average scattering density is assumed to be the same in the two types of blocks, which is a good approximation in the present case. The construction of the diffraction pattern using this method is shown in Fig. 10b. The semiquantitative agreement with the observed diffraction pattern of Fig. 3a is quite satisfactory, proving that the diffraction pattern is produced by the above-mentioned sequence.

Keeping in mind that the crystallographic shear planes are the principal planar defects observed in the high-resolution images, the diffraction pattern of Fig. 3c can also be interpreted. As was shown in Fig. 1, the displacement vector of the crystallographic shear planes is $\mathbf{R} = \frac{2}{3}[101]$. One-dimensional disorder due to interfaces with a displacement vector $\mathbf{R}$ causes all reflections for which $\mathbf{g} \cdot \mathbf{R}$ is not integer to be streaked. In the present case with $\mathbf{R} = \frac{2}{3}[101]$ one finds $\mathbf{g} \cdot \mathbf{R} = \frac{2}{3}(h + l)$. Since, moreover, the diffraction condition $h + l = 2n$ has to be satisfied because the lattice is body centered, one finds that spots with $h + l = 6$-fold remain sharp, which is clearly the case in Fig. 3c. This shows that in certain crystal fragments, disordered arrays of crystallographic shear planes are present.

5.2. *Diffuse Scattering*

The diffuse scattering appearing in Figs. 1b and 1c can be interpreted using the direct method developed in (19).

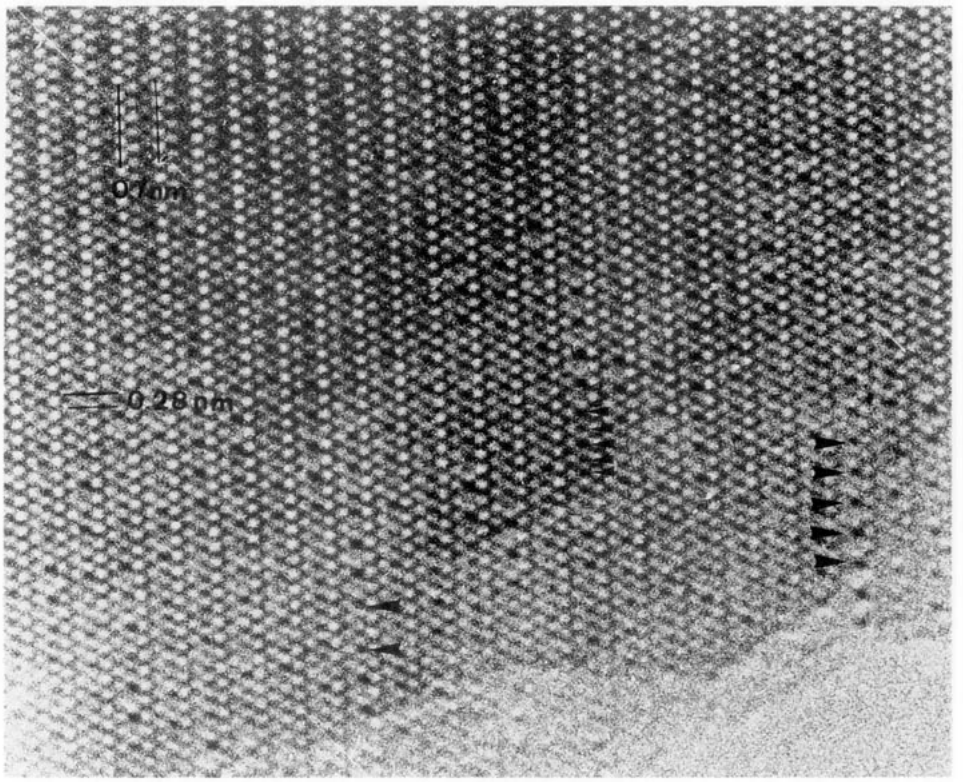

FIG. 7. High-resolution image along the [11$\bar{1}$] zone parallel to the barium columns. The dark dots image the barium columns. Small arrowheads indicate separations of b_m, while larger arrowheads indicate separations of $2b_m$ and $3b_m$.

The equation of the planes of diffuse scattering can be formulated as $\sin 2\pi k = 0$. The zeros of this function occur for $k = (\frac{1}{2})n$, where n is an integer. This relation represents the observed planes of diffuse scattering. The locus of diffuse scattering is directly related to the state of order of the different sublattices, which is described by a "cluster relation" defined in the mentioned reference. In the present case the cluster consists of two sites related by a vector $2b_m$, and the cluster relation states that all pairs of such sites should be occupied either both by the same atom species, or both by vacancies. Since b_m is a symmetry translation for the MnO_2 framework, the cluster relation is automatically satisfied for the Mn and the O sublattices. However, it does restrict the configuration of Ba atoms which should be separated by $2b_m$ along the channel; no other restrictions are imposed by the diffuse scattering locus, which means that there is no correlation between the "phase" of the arrangement in different channels. It is clear that this is consistent with the interpretation of the high-resolution images.

Occasionally, in oblique sections of the reciprocal space, several diffuse lines perpendicular to the [010]* direction have been observed. Figure 11 shows such a diffraction pattern revealing several (0k0)* levels of sharp spot rows. Between the rows of sharp spots, three weak parallel lines of diffuse intensity can be distinguished. The central line, midway at $\frac{1}{2}(010)^*$ between the rows of spots, is the best observable one. The other two weaker lines divide the distance between the sharp spot rows in three equal parts. From tilting experiments we concluded that the lines correspond with diffuse planes at $\frac{1}{3}(010)^*$ and at $\frac{2}{3}(010)^*$. This observation confirms the presence of phase uncorrelated strings of channel ions spaced by $2b_m$, and also shows that in certain parts of the sample, the interionic spacing in the strings can also be $3b_m$. The high resolution image in Fig. 7 shows that in certain areas such a separation of dark dots is also possible (indicated).

5.3. *Image Simulations*

In order to support the interpretation of the black dots in Fig. 7, images were computer simulated using the software package "Mac Tempas." The model was based on the normal structure described above, in which half of the rows of the barium ions were removed, resulting in a periodic structure in which the spacing between the barium ions in the channel is $2b_m$. This model was postulated because it was suspected that the black dots reveal the barium arrangement in the channels. Some relaxation of approximately 2% in the interatomic distances was

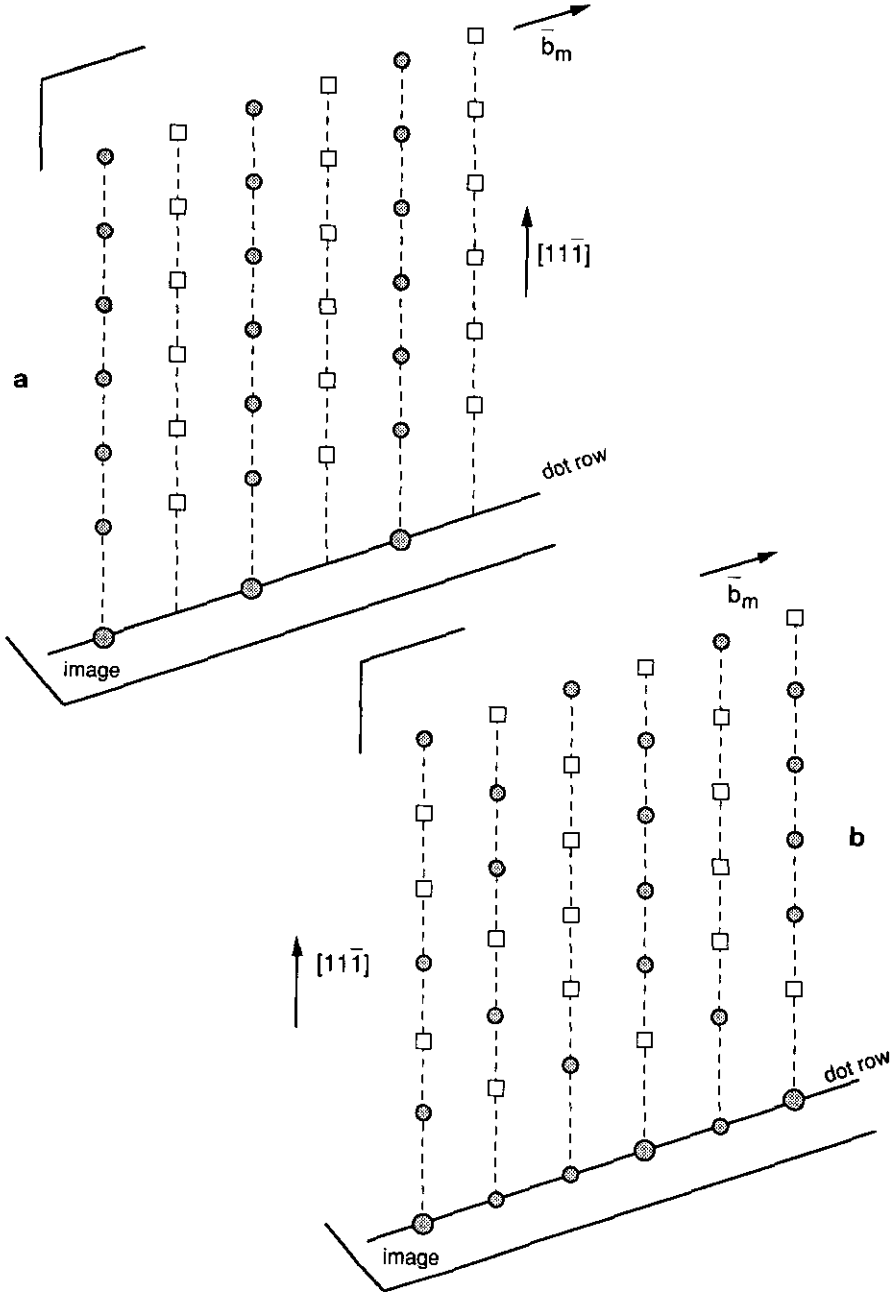

FIG. 8. Schematic representation of the Ba ions in the channels along b_m: (a) every other channel is occupied; (b) random occupation.

allowed for by moving the adjacent manganese ions toward the centers of the positively charged barium vacancies and moving the oxygen atoms away from these centers. The resulting simulated images along the [11$\bar{1}$] zone are shown in Fig. 12. The following values were assumed for the image parameters: spherical aberration constant C_S = 1 mm, beam divergence θ = 0.55 mrad. The foil thickness was varied from 3 to 9 nm and the defocus values were varied in steps of 10 nm. The objective aperture was 0.07 nm^{-1}. The best fit with the observed image (Fig. 7) was obtained for a foil thickness Δt = 6 nm and a defocus value of $\Delta f = -10$ nm. The black dots indicated by arrowheads in Fig. 12 correspond to barium positions, confirming that the interpretation of the black dots in Fig. 7 as images of barium columns is justified.

6. PHASE TRANSITION

As we have already suggested, the monoclinic structure of hollandite could be formed by a phase transition from

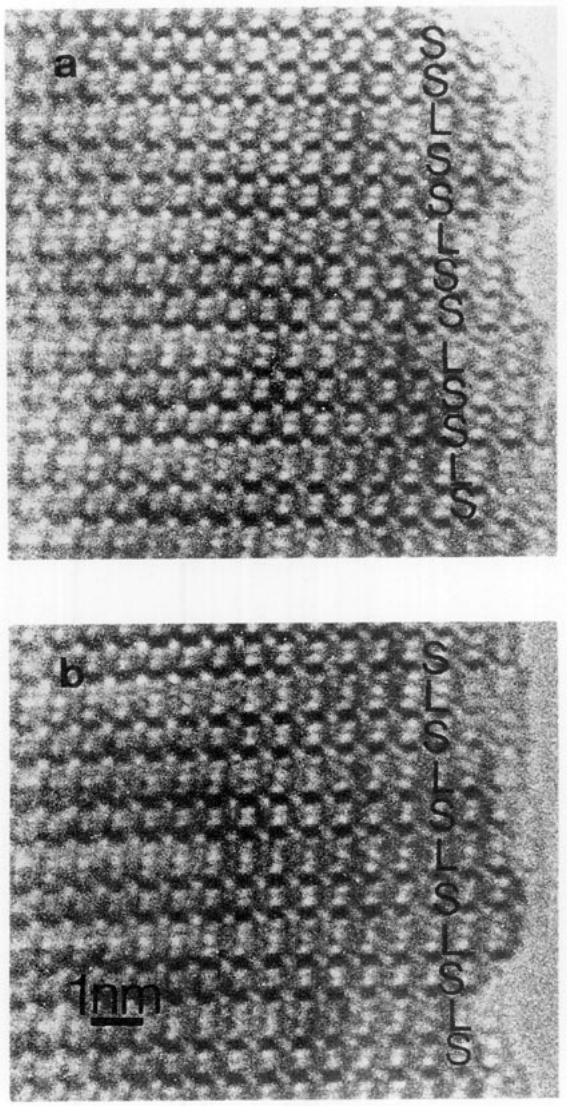

FIG. 9. High-resolution image along the [010] zone showing regular successions of long (L) and short (S) blocks due to periodic shear structures: (a) ... *LSSLSS* ... sequence; (b) ... *LSLSLS* ... sequence.

the higher temperature tetragonal phase by deformation of MnO_6 octahedra. The resulting variants would then be related by the lost symmetry operation, which is a rotation of 90° about the fourfold axis.

Since at room temperature the natural $Ba_xMn_8O_{16}$ studied in this paper was monoclinic, we have performed *in situ* heating of the sample using the heating stage of the electron microscope. It is worth mentioning that direct heating by the 400 kV-electron beam did not produce significant changes during the observation time.

The monoclinic to tetragonal transition in a synthetic hollandite was previously studied by Cheary (3). In this case, the sample was of the SYNROCK type ($Ba_x[Ti_\alpha Al_{1-\alpha}]Ti_{8-2x}O_{16}$), and the transition was observed by means of X-ray diffraction.

Figure 13 gives a set of electron diffraction patterns of the [010] zone obtained on the same crystallite at different temperatures. We have chosen this orientation because the major changes of the cell shape on transition are expected to occur in the (010) plane, where the monoclinic distortion is directly revealed.

Figure 13a shows the diffraction pattern at room temperature. The image reveals the splitting of the diffraction spots due to twinning as in Fig. 2a. As the temperature increases gradually (Figs. 13b and 13c), the spot splitting decreases and finally disappears at a temperature of approximately 330°C, where the structure becomes tetragonal, Fig. 13c. It should be mentioned that because of the errors in measuring the temperature we can determine only approximately the transition temperature. These errors are possibly due to bad thermal contact of the sample and possibly to supplementary heating by the electron beam, since the thermocouple of the microscope heating

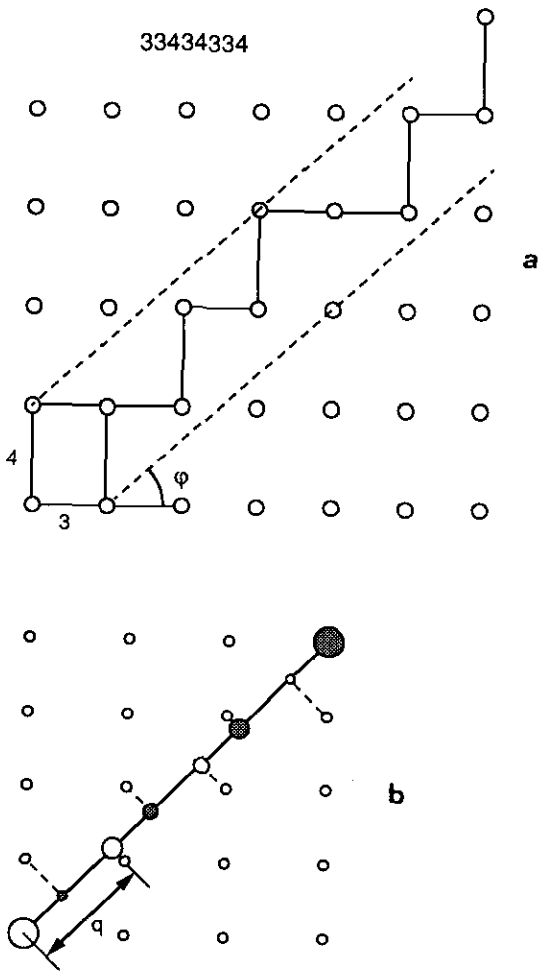

FIG. 10. Geometric construction used to obtain (a) the stacking sequence of long (L) and short (S) blocks, and (b) the diffraction pattern.

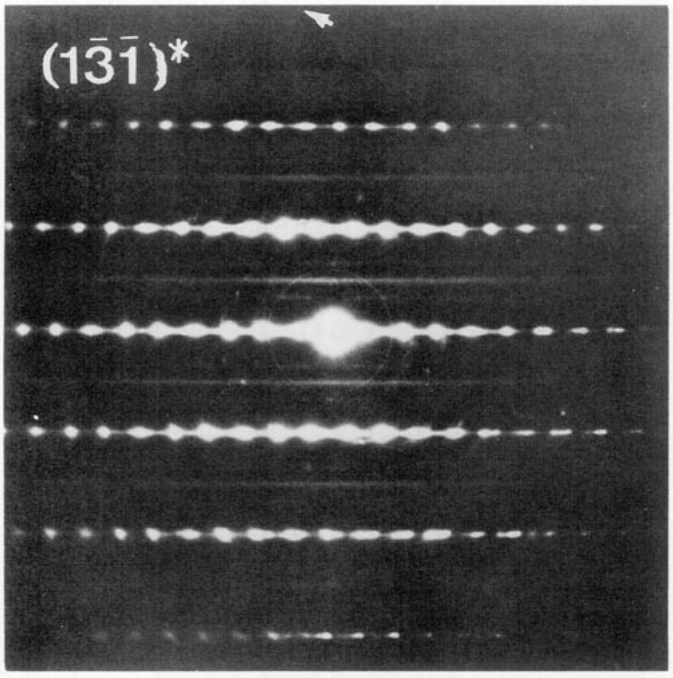

FIG. 11. Oblique section in the reciprocal space revealing three diffuse lines perpendicular to the projected [010]* direction. The diffuse lines correspond to planes at $\frac{1}{2}(010)^*$, $\frac{1}{3}(010)^*$, and $\frac{2}{3}(010)^*$.

holder measures the furnace temperature, and not that of the sample.

Figure 14 represents the variation of the lattice parameters a, c, and β of the monoclinic phase as a function of temperature. The lattice parameters converge continuously and monotonously to the tetragonal values $a = c$ and $\beta = 90°$. This shows that during heating the changes of the MnO_6 octahedra occur gradually as a relaxation of the shear strain in the channel walls (3), which was introduced by the monoclinic deformation.

The diffraction pattern of the $Ba_xMn_8O_{16}$ crystallite after cooling again to room temperature is reproduced in Fig. 13d. One can note that this diffraction pattern is rotated over 90° as compared with the initial orientation (Fig. 13a), confirming that the crystallite has been in the tetragonal phase. The final lattice parameters are slightly different from the initial ones: $a = 1.037$ nm, $c = 1.06$ nm, $\beta = 91.5°$, as compared to $a = 1.037$ nm, $c = 0.985$ nm, $\beta = 91.5°$, showing that on fast cooling the deformation of the MnO_6 octahedra at the transition to monoclinic phase was also slightly different. This can be explained by considering that natural hollandite contains water as molecular H_2O and OH^- (12, 15). The H_2O molecules fill some of the channel sites while OH^- substitutes for O^{2-}. During the heating of the sample, the water molecules might be

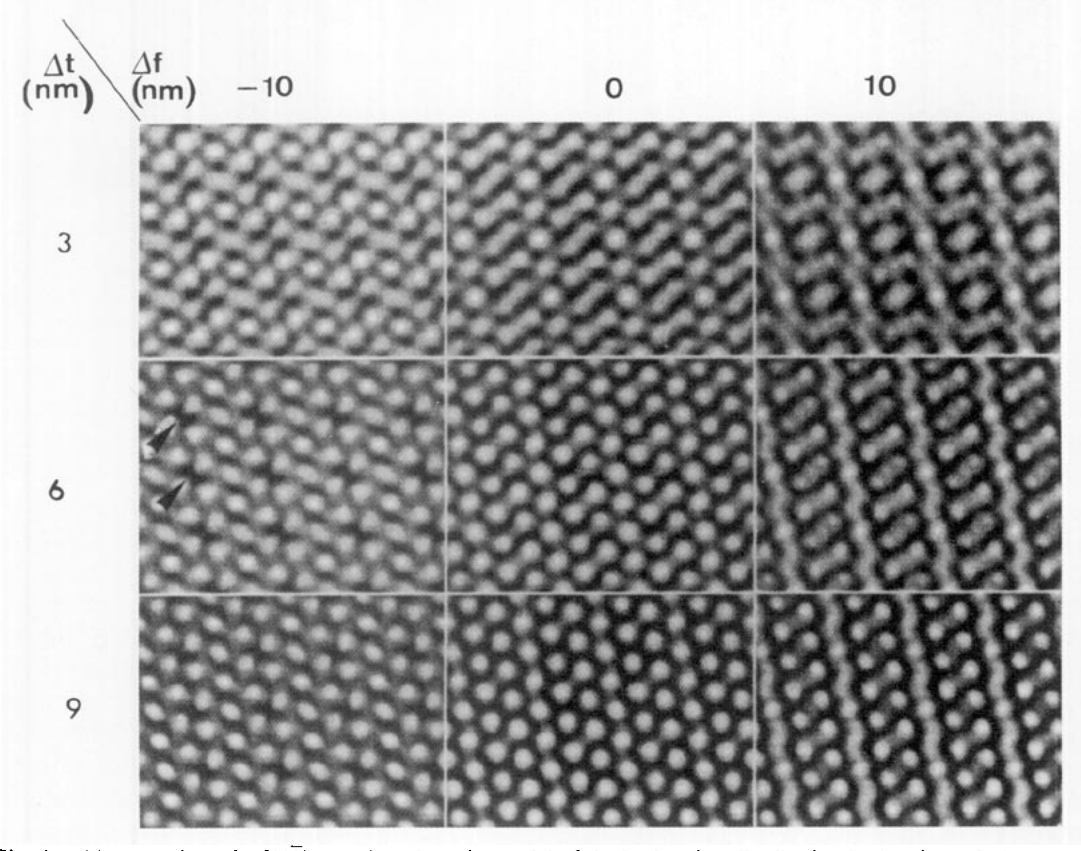

FIG. 12. Simulated images along the [11$\bar{1}$] zone based on the model of the barium ion distribution in the channels (see text). Defocuses and thicknesses for the various images are indicated in nm.

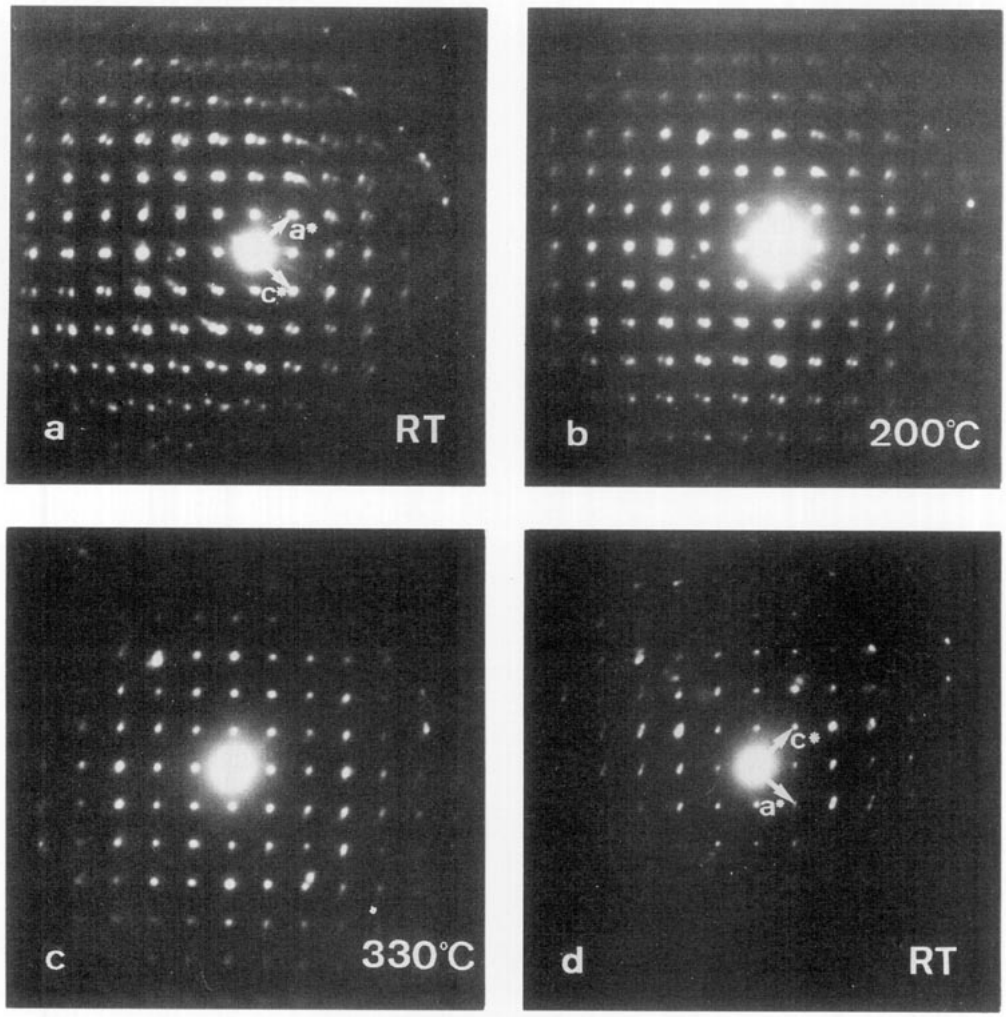

FIG. 13. A set of diffraction images of the [010]* zone taken at different temperatures, revealing the monoclinic to tetragonal phase transition: (a) room temperature; (b) 200°C; (c) 330°C; (d) room temperature after cooling.

lost in the microscope vacuum, leaving empty sites in the structure channels. The deformation of the channel walls at the tetragonal–monoclinic transition will then be slightly influenced.

7. DISCUSSION AND CONCLUSIONS

Using high resolution imaging it has been demonstrated that the spacing between the barium ions which occupy the simple channels (2 × 2 octahedra) in natural holandite is preferentially $2b_m$, but that also $3b_m$ spacings occur. Moreover, it is found that the arrangements in neighboring channels are only weakly correlated. The loss of correlation is directly related to the nonstoichiometry which causes the occurrence of singular ion–ion spacings of $3b_m$ within the same channels containing predominantly sequences of spacing $2b_m$. Such a singular spacing causes neighboring arrangements to become out of step and thus give rise to "pencil" disorder of the barium strings.

The existence of interfaces consisting of larger rectangular (3 × 2 octahedra) channels leads to an additional possibility to accommodate nonstoichiometry, since these layers can be considered as crystallographic shear planes. The rectangular channels are occupied by barium ions almost certainly in a staggered configuration, leading to about the same average separation of the barium ions along [010] as in the simple square channels. Since more MnO_6 octahedra are involved in the formation of a rectangular channel than are necessary for a simple square channel, the net effect of introducing shear planes may be a decrease in the average barium concentration.

The uniform but nonperiodic arrangement of layers of square and rectangular channels leads to structural variants which in some cases produce apparently incommen-

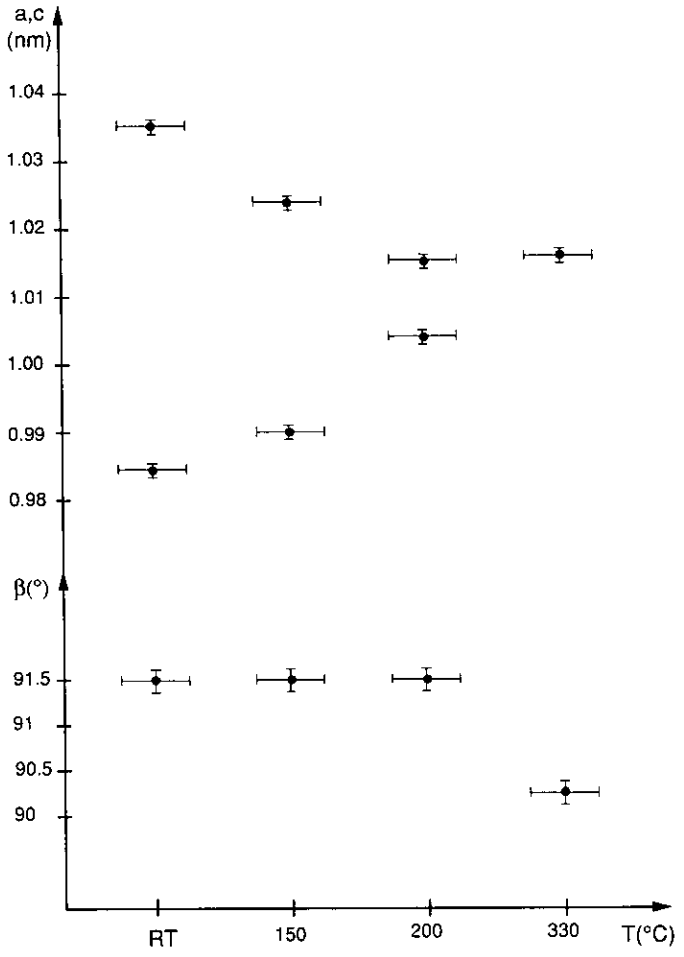

FIG. 14. Lattice parameters plotted as a function of temperature.

surate diffraction patterns (Figs. 3a and 3b). Sequences of regular periodic arrangements are usually only short; they do not produce a characteristic diffraction pattern, but high resolution electron microscopy allows us to reveal these local phases.

In synthetic hollandites layers of rectangular channels of similar type are a feature of the normal structure. It is therefore not surprising to find such layers as defects in the present material.

Also, large square channels (3 × 3 octahedra) are formed along the intersection line of two layers of rectangular (3 × 2 octahedra) channels (Fig. 6). Along such channels the barium ions are most probably arranged helically, since this maximizes their separation for a given concentration. The resulting ion–ion separation is not very different from that in the small channels; hence such singular channels lead again to a small decrease of the barium concentration.

The high resolution images along [010] have made it possible to reveal heavy atom columns and in particular to visualize the pattern of manganese columns forming the channel walls and exhibiting deviations from tetragonal symmetry. With increasing temperature the tetragonal symmetry is recovered at about 330°C. This suggests that the monoclinic deformation is presumably caused by the cooperative deformation of the MnO_6 octahedra. These would become regular at the transition temperature. The deformation of the octahedra can apparently occur in two different ways, producing twin related structures. On cooling again after having been transformed into the high-temperature tetragonal phase, the monoclinic phase can form in two variants; a given domain may therefore possibly transform into the other twin variant. This is apparently what happened in the sample that produced the sequence of diffraction patterns of Fig. 13; it shows that the specimen passed through the tetragonal phase.

ACKNOWLEDGMENT

One of us (L.C.N.) is indebted to the Belgian Government, Prime Minister's Office of Science Policy Programming for her fellowship at the University of Antwerp (RUCA).

REFERENCES

1. R. W. Cheary, *Acta Crystallogr., Sect. B* **42,** 229 (1986).
2. R. W. Cheary, and R. Squadrito, *Acta Crystallogr., Sect. B* **45,** 205 (1989).
3. R. W. Cheary, *Acta Crystallogr., Sect. B* **46,** 599 (1990).
4. L. A. Bursill and D. J. Smith, *J. Solid State Chem.* **69,** 343 (1986).
5. F. C. Mijlhoff, D. J. W. Ijdo, and H. W. Zandbergen, *Acta Crystallogr., Sect. B* **41,** 98 (1985).
6. L. A. Bursill and G. Grzinic, *Acta Crystallogr., Sect. B* **36,** 2902 (1980).
7. A. Pring, D. J. Smith, and D. A. Jefferson, *J. Solid State Chem.* **46,** 373, (1983).
8. H. W. Zandbergen, P. L. A. Everstijn, F. C. Mijlhoff, G. H. Renes, and D. J. W. Ijdo, *Mater. Res. Bull.* **22,** 431 (1987).
9. J. Vicat, E. Fanchon, P. Strobel, and D. T. Qui, *Acta Crystallogr., Sect. B* **42,** 162 (1986).
10. E. Fanchon, J. Vicat, J. L. Hodeau, P. Wolfers, D. T. Qui, and P. Strobel, *Acta Crystallogr., Sect. B* **43,** 440 (1987).
11. T. Vogt, E. Schweda, C. Wüstefeld, J. Strähle, and A. K. Cheetham, *J. Solid State Chem.* **83,** 61 (1989).
12. A. Byström and A. M. Byström, *Acta Crystallogr.* **3,** 146 (1950).
13. A. Byström and A. M. Byström, *Acta Crystallogr.* **4,** 469 (1951).
14. B. Mukherjee, *Acta Crystallogr.* **13,** 164 (1960).
15. J. E. Post, R. W. Von Dreele, and P. R. Buseck, *Acta Crystallogr., Sect. B* **38,** 1056 (1982).
16. S. Andersson and A. Wadsley, *Nature* **211,** 581 (1966).
17. D. Frangis, S. Kuypers, C. Manolikas, G. Van Tendeloo, J. Van Landuyt, and S. Amelinckx, *J. Solid State Chem.* **84,** 314 (1990); G. Van Tendeloo, C. Van Heurck, and S. Amelinckx, *Solid State Commun.* **71,** 705 (1989).
18. V. Elser, *Phys. Rev. B* **22,** 4892 (1985); *Acta Crystallogr., Sect. A* **42,** 36 (1986); D. Levine and P. J. Steinhardt, *Phys. Rev. Lett.* **53,** 2477 (1984); *Phys. Rev. B* **34,** 596 (1986); M. Duneau and A. Katz, *Phys. Rev. Lett.* **54,** 2688 (1985).
19. S. Amelinckx, *in* "Materials Science and Technology—A Comprehensive Treatment" (R. V. Cahn, P. Haasen, and E. J. Kramer, Eds.), Vol. 2A, p. 106. VCH, New York, Weinheim, Basel, 1993.